Kinetic-energy-driven enhancement of secondary-electron yields of highly charged ions impinging on thin films of C_{60} on Au

E. Bodewits* and R. Hoekstra†
KVI–Atomic and Molecular Physics, University of Groningen, Zernikelaan 25, 9747 AA Groningen, The Netherlands

K. Dobes and F. Aumayr
Institute of Applied Physics, TU Wien–Vienna University of Technology, A-1040 Vienna, Austria
(Received 9 November 2012; published 20 December 2012)

The secondary electron yields as a result of slow highly charged ions (Ar^{4+},Ar^{13+}) impinging on clean Au(111), highly oriented pyrolitic graphite, and thin films of C_{60} on Au are presented. In order to investigate the dynamics of the neutralization of the highly charged ions in front of the surface, angular scans have been performed. The results give a clear indication that the observed increase in electron yield seen on C_{60} compared to Au stems from kinetic-energy-driven processes and not from processes driven by the potential energy carried by the highly charged ion.

DOI: 10.1103/PhysRevA.86.062904 PACS number(s): 79.20.Rf, 34.70.+e

I. INTRODUCTION

The neutralization of slow highly charged ions (HCIs) at surfaces is dominated by resonant processes leading to the formation of transient so-called hollow atoms, i.e., atoms with populated outer shells and empty inner shells [1–3]. The hollow-atom creation and its consecutive decay has been studied extensively by a large variety of experimental techniques. The initial phases, creation and decay in front of the surface are well-described by the classical over-the-barrier (COB) model [4]. For metallic targets the target enters into the COB model description via its work function. For nonmetallic targets the binding energy of the least bound electrons determines mainly the distance of first capture [5]. Thin films have been used to make a smooth gradual transition from a metallic to an insulator surface [6–9].

In a previous paper we presented work on C_{60} evaporated on Au [10]. Following the COB model, the first capture distance of electrons is closer to the surface for C_{60} than for Au. This suggests that there is less time available for relaxation of the hollow atoms by means of Auger decay before they penetrate the surface. In addition, because of the resonant nature of the electron capture, lower-lying, more strongly bound states in the hollow atom get populated, which is likely to imply that fewer Auger steps are necessary for the full relaxation of the hollow atoms. On the basis of these arguments one is inclined to expect that less secondary electrons will be emitted for C_{60} films on Au than for clean Au. However, it turned out that when Ar^{q+} (with $q = 7$–13) and Xe^{q+} (with $q = 10$–26) ions impinge under 45° on thin films of C_{60} the secondary electron yield emission is actually approximately 30% larger than for a clean Au(111) surface.

Several scenarios which might explain the increase in secondary electron yield are available. Recently the original over-the-barrier model was extended by Lake *et al.* [11] by the inclusion of a thin dielectric film on top of a metal surface. An HCI approaching the film may perturb the thin film such that throughout the film the bottom of its conduction band drops below the work function of the substrate, while the barrier between the HCI and the thin film is still high enough that over-the-barrier transitions between the film and the HCI are not yet possible. In this way the dielectric film appears to lower the substrate's work function. The earlier onset of the neutralization and creation of hollow atoms will give more time in front of the surface for the relaxation processes of hollow atoms. Meyer and coworkers showed that upon decreasing the work function of a gold surface by means of evaporating Cs, the above-surface K Auger component increased by as much as 30%, which could be linked to more time available above the surface [12].

Another scenario for the increase in the secondary electron yield is the larger escape length of electrons produced below the surface for C_{60}, which in part may be counteracted by the lower electron density. Thin films of C_{60} have a very open structure, therefore electrons produced in the C_{60} film may have a higher probability of escaping and being detected. Cernusca and coworkers used singly charged ions on differently oriented highly oriented pyrolytic graphite (HOPG) samples [13]. For HOPG with its planes oriented normal to the surface, the electron yield is twice as high as when the planes are oriented parallel to the surface. The explanation is that the electrons have a much larger mean escape depth for the HOPG oriented normal to the surface.

In this paper we present the angular dependency of secondary electron yields resulting from HCIs interacting with clean gold thin films of C_{60} and HOPG. The results presented mainly focus on Ar^{13+} and Ar^{4+} ions with kinetic energies in the range of 1–100 keV. First, some general features of electron emission are studied in clean Au. Then the same method is applied to thin films of C_{60} to investigate the hollow atom decay at insulators.

II. EXPERIMENTAL SETUP

The experiments were performed in the experimental setup IISIS (Inelastic Ion Surface Interaction Station). IISIS [14] is constructed as a future user station at the HITRAP [15]

*ebodewits@kvi.nl
†hoekstra@kvi.nl

facility at the Helmholtz Zentrum GSI (Darmstadt, Germany). The experimental setup IISIS is described in more detail in Refs. [10] and [14]. The base pressure in the main chamber is in the 10^{-11} mbar regime and kept there by means of a 400 L/s ion pump. During the measurements the pressure is in the 10^{-10} regime and kept there by a 360 L/s turbo pump, while the ion pump is switched off in order not to interfere with the secondary electron statistics measurements.

Ions are transported through a set of diaphragms and interact with the sample mounted on a VG Scienta manipulator equipped with a home-built sample holder. The present design of the sample holder assures that the ion beam does not interact with the support material. The sample can be rotated over 360° and moved in the X, Y, and Z directions.

The Au(111) target used in the present experiments is prepared by cycles of sputtering with 7-keV Ar^+ ions under grazing incidence angles and annealing at temperatures of up to 500° C. The surface composition is checked by means of time-of-flight low-energy ion scattering. The HOPG target is prepared by means of the Scotch tape cleaving method, which produces clean and atomically flat surfaces.

The electron statistics detector [16–18] is mounted under 90° with respect to the incoming beam. To collect all the emitted electrons on the electron statistics detector, the sample is surrounded by five electrodes. Four of the electrodes are biased negatively to optimize the electron collection efficiency. The fifth electrode, a highly transparent grid mounted directly in front of the electron statistics detector, is biased positively to attract electrons. This assures the collection of all the emitted electrons. The electron number statistics detector itself is further described in [14], [19], and [20], and references there in.

When using low-energy ion beams, the electrodes have an undesired side effect: the positive biased grid is pushing the ion beam away from the detector, thereby changing the incidence angle of the ion beam on the surface. For ion beams with a kinetic energy of 2 keV/q or higher the effect is below 2° (cf. Fig. 1). For ion beams with a lower kinetic energy a correction $\Delta\psi$ needs to be applied to the incidence angle ψ'. To account for this the change in incidence angle has been determined by SimIon simulations [21]. Here, for various incidence angles ($\psi' = 10°$, 30°, and 60°) and energies (0.25–7 keV/q) the real incidence angle ψ has been determined. Figure 1 shows the result of the simulations. Since the target holder is relative small compared to the rest of the chamber, the electric fields are barely affected by the polar angle of the sample itself, which is on ground potential. Therefore, the angular correction angle which needs to be added to the incidence angle set in the experiment is almost angular independent. As mentioned earlier, the correction in angle is small for ions with an energy higher than 2 keV/q, but for ions with a kinetic energy of 0.5 keV/q the change is as high as 10°. In the results presented below, the angular correction has been applied when appropriate.

The deposition of thin films of C_{60} is done using an Omicron EFM 3 evaporator. The evaporator has a built-in flux monitor to monitor and control the outgoing particle flux. The evaporation of the C_{60} is done by means of electron bombardment heating of a crucible containing C_{60} powder (99.9% pure; Sigma-Aldrich). The deposition rate is monitored by a quartz microbalance (Tectra, type MTM-EK). The microbalance is mounted on a linear translation stage to position the quartz crystal at the same site where the sample is mounted during evaporation. Using the quartz microbalance, it is possible to measure deposited mass amounts equal to a small fraction of a monolayer (ML). For a more detailed description regarding the evaporation of C_{60} see Ref. [10].

III. RESULTS

In order to assess the effect of C_{60} films on the secondary electron yields, first reference measurements were performed on clean Au(111). Figure 2 shows the secondary electron yield γ obtained with Ar^{4+} and Ar^{13+} impinging on clean gold as a function of the incidence angle. The kinetic energies shown

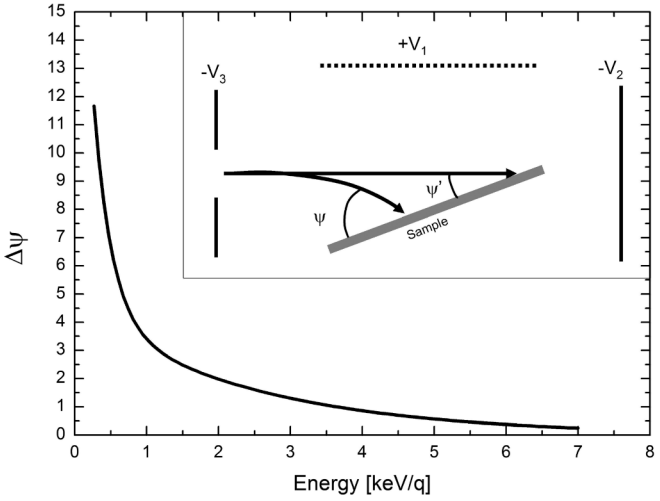

FIG. 1. Values obtained for $\Delta\psi$ ($\Delta\psi = \psi - \psi'$) from SimIon as a function of the kinetic energy of the ions. Inset: Sketch and definition of ψ' and ψ. $V_{1,2,3}$ are the potentials applied to assure maximum collection efficiency.

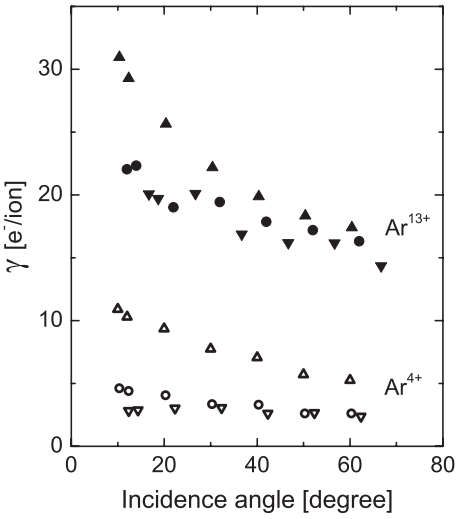

FIG. 2. The electron yield as a function of the incidence angle for three kinetic energies—91 keV (upward-pointing triangles), 28 keV (circles), and 6.5 keV (downward-pointing triangles)—for Ar^{4+} and Ar^{13+} on Au(111).

are 6.5, 28, and 91 keV. For Ar^{13+} the secondary electron yield is higher than for Ar^{4+}, which is due to the higher potential energy carried by the Ar^{13+} ion [14,22–25].

The second feature visible is the increase in electron yield as a function of the kinetic energy. For 6.5 and 28 keV the yields are almost the same due to the fact that these energies are below or close to the threshold for kinetic electron emission, which, for Ar ions impinging on Au, lies around 16 keV [23]. The electron yields for 91 keV $Ar^{4,13+}$, however, are clearly higher. The increase is due to kinetic electron emission.

The last feature of relevance for the further discussion is the increase in the secondary electron yield for more grazing angles of incidence. There might be two grounds for this

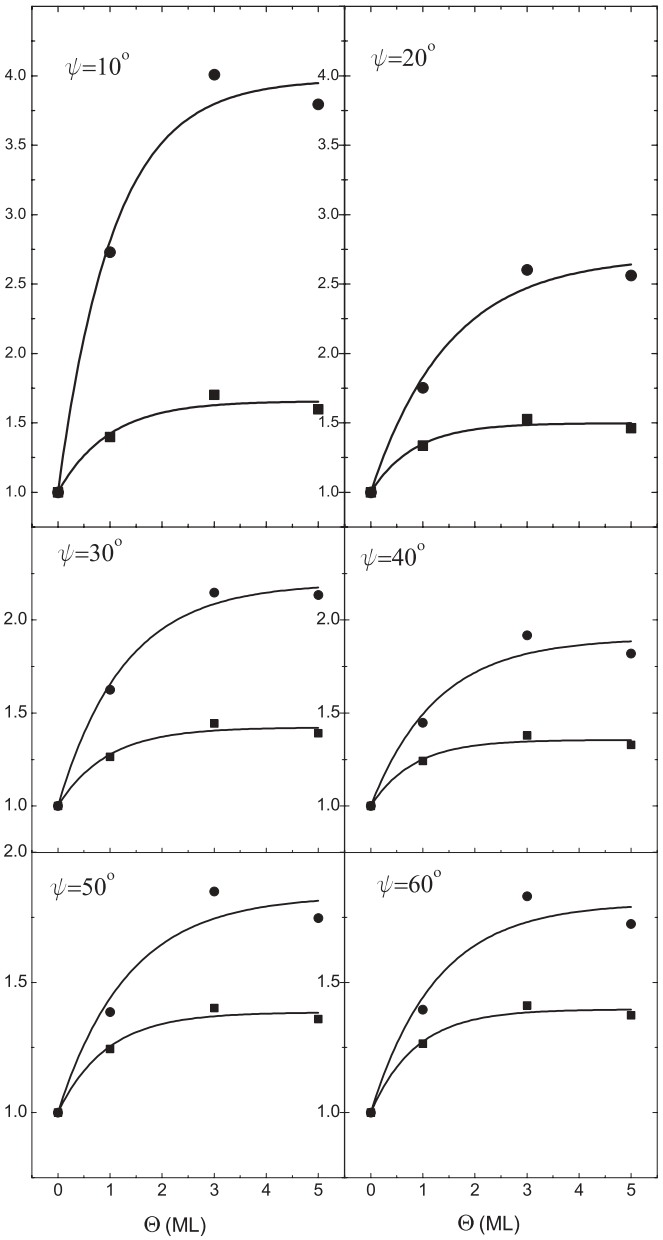

FIG. 3. Relative secondary electron yield $\gamma_{rel}(\Theta)$ as a function of ML thickness for 28-keV Ar^{4+} (filled circles) and Ar^{13+} (filled squares) ions at different incidence angles. Curves represent fits to data based on Eq. (2).

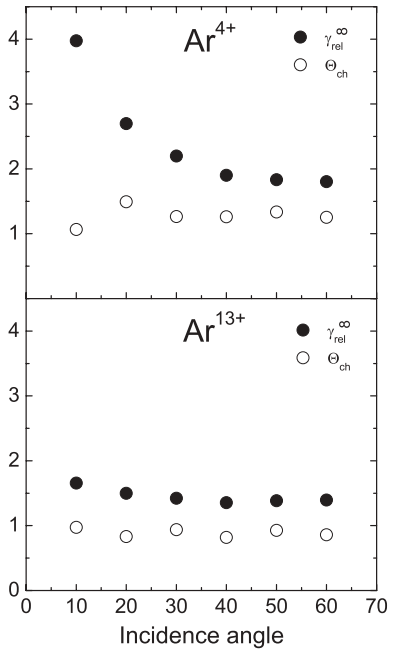

FIG. 4. Values of the fitting parameters γ_{rel}^{∞} and Θ_{ch} [Eq. (2)] for 28-keV Ar^{4+} and Ar^{13+} impinging on Au/C_{60}.

increase. At smaller incidence angles the time between first capture and impact on the surface increases and after impact the trajectory path length of the projectiles just below the surface gets longer, and thus more electrons produced below the surface can escape from the target.

When thin films of C_{60} are evaporated on gold, the electron yield increases. In order to compare this increase in secondary electron yield for differently charged ions, i.e., Ar^{4+} and Ar^{13+}, the secondary electron yield relative to the clean Au case, γ_{rel}, is introduced by

$$\gamma_{rel}(\Theta) = \frac{\gamma^{C_{60}}(\Theta,\psi)}{\gamma^{Au}(\Theta=0,\psi)}. \quad (1)$$

Here, Θ is the number of MLs of C_{60}, $\gamma^{C_{60}}(\Theta,\psi)$ the yield measured on Θ MLs of C_{60}, and $\gamma^{Au}(\Theta=0,\psi)$ the yield measured on clean gold. Figure 3 shows the relative yield for six incidence angles, ranging from 10° to 60°, for 28-keV Ar^{q+} with $q = 4$ and 13. For all angles measured, the increase in the relative yield, γ_{rel}, is higher for Ar^{4+} than for Ar^{13+}. For low incidence angles this is most obvious. As proposed in a previous paper [10], the relative yield is represented by an exponential gain curve, given by the equation

$$\gamma_{rel}(\Theta) = \gamma_{rel}^{\infty} - (\gamma_{rel}^{\infty} - 1)e^{-\Theta/\Theta_{ch}}, \quad (2)$$

with γ_{rel}^{∞} the relative yield for very thick layers, i.e., bulk C_{60} and Θ_{ch}, a characteristic layer thickness. In Fig. 3 the corresponding fits to the data are included for each incidence angle. The associated values of the parameters γ_{rel}^{∞} and Θ_{ch} are shown in Fig. 4.

IV. DISCUSSION

At all angles of incidence investigated the data for 28-keV Ar^{4+} and Ar^{13+} ions show an increasing secondary electron yield when evaporating C_{60} films on the Au substrate

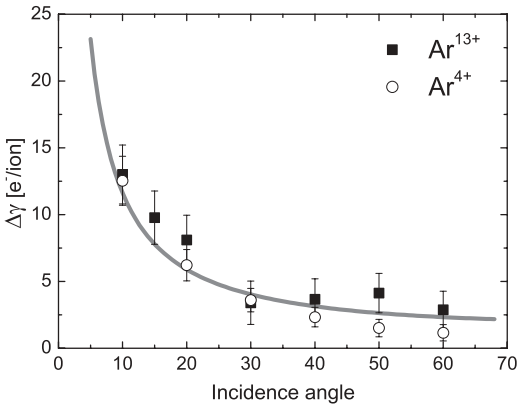

FIG. 5. Difference in absolute yield between 5-monolayer C_{60} and Au for 28-keV Ar^{13+} (filled symbols) and Ar^{4+}. The fit is proportional to $\sin^{-1}(\psi)$.

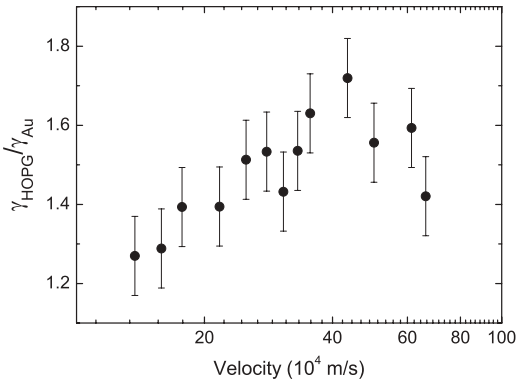

FIG. 6. The relative electron yield for HOPG with respect to Au as a function of the kinetic energy for Ar^{13+} ions.

surface. The enhancement is strongest at smaller angles of incidence and is much stronger for Ar^{4+} than for Ar^{13+}. The characteristic layer thickness seems to be independent of the angle of incidence (cf. Fig. 4). For Ar^{4+} the characteristic layer thickness is approximately 1.3 MLs, while for Ar^{13+} the thickness falls just below 1 ML. This means that most of the enhancement of the electron emission takes place above or in the first ML of C_{60}. The value of $\gamma_{\mathrm{rel}}^{\infty}$ seems to be almost incidence angle independent for Ar^{13+} but shows a strong increase for Ar^{4+} upon decreasing the incidence angle. For a 10° incidence angle, the enhancement of the relative yield goes up to a factor of 4.

In order to figure out the reason for this strong increase, the absolute electron yields were investigated. Here we focus on the difference in absolute electron yield between 5 MLs of C_{60} and clean Au(111) for Ar^{4+} and Ar^{13+} ions. As shown in Fig. 5, the difference in absolute electron yields between the electron yield measured on 5 MLs of C_{60} and clean Au is the same for Ar^{4+} and Ar^{13+} ions. This explains why the relative increase for Ar^{4+} is much higher than that for Ar^{13+}. Since the absolute change in electron yield is the same for both ions, it seems unlikely that the increase in the electron yield is due to potential emission. It rather suggests that the kinetic energy of the ion must be responsible for the yield increase. For kinetic electron emission the electron yield follows a relation close to $\sin^{-1}(\psi)$, which is well known by now and used in, for example, helium ion microscopes [26]. When fitting the difference in absolute yield to this relation it is shown (Fig. 5) that there is a good agreement with the $\sin^{-1}(\psi)$ relation.

This supports the idea that the enhancement is due to kinetic electron emission. For Ar ions impinging on Au the threshold for kinetic emission is ∼16 keV [23]. At the energy used, 28 keV, the kinetic electron emission is still very weak (∼1 electron/ion at 90° [23]). This can also be inferred from the small increase in secondary electron yields for both Ar^{4+} and Ar^{13+} ions when changing the kinetic energy from 6.5 keV (well below the kinetic threshold) to 28 keV (see Fig. 2).

For the C_{60} layers the threshold for kinetic electron emission must be much lower than the one for Au to realize the observed enhancement of the electron emission. No information is available about the kinetic emission threshold of thin films of C_{60},or on bulk C_{60}.

However, for HOPG, another graphite material, kinetic electron emission experiments have been performed by Cernusca *et al.* [13]. In their experiments, they found a threshold for the kinetic electron emission of only 4 keV and a linear increase in electron yield as a function of velocity [27]. Comparing the kinetic electron emission of Ar^{+} ions impinging on HOPG and Au [23], except for velocities very close to the kinetic threshold, one finds that the slopes of the kinetic electron emission yields are almost the same.

Using this information and assuming that the potential electron emission is more or less constant over the energy range investigated, it is now possible to sketch the general behavior one would expect for the ratio between electron yields on HOPG and Au ($\gamma_{\mathrm{HOPG}}/\gamma_{\mathrm{Au}}$). Below the kinetic threshold velocity of HOPG, the ratio will be constant. When kinetic electron emission starts to play a role for HOPG and not yet for Au, the ratio is expected to increase. The electron yield ratio is then expected to decrease again for high velocities exceeding the kinetic threshold of Au. Figure 6 shows the electron yield ratio of HOPG and Au as a function of the velocity of the Ar^{13+} ions. The lowest velocity (kinetic energy of 4 keV) corresponds to the kinetic emission threshold of HOPG. From 4 keV on, there is a gradual increase in relative electron yield. After reaching a maximum between 30 and 40 keV, the relative yield goes down again, as expected from the scenario described above. Therefore it seems that indeed the difference in kinetic threshold energies is responsible for the increase in the relative electron emission yields.

The similarity between HOPG and C_{60} can be assessed on the basis of their respective secondary electron yields. The electron yields measured with Ar^{13+} on Au, 5 MLs of C_{60}, and HOPG are compared in Fig. 7. For low kinetic energies, around the threshold of HOPG (4 keV), the electron yields on Au and C_{60} are the same. This suggests that the potential emission is the same for C_{60} and Au. For HOPG, however, it seems that the electron yield is somewhat higher. A possible reason for this higher electron yield is that there are still some kinetic electrons in the case of HOPG, while for C_{60} possibly the threshold lies somewhere between that of Au and that of HOPG. Probably the escape depth of the electrons plays a role here too: for slow ions penetrating a surface, a larger fraction of the decay processes takes place relatively close to the surface than for ions with a higher impact velocity. The

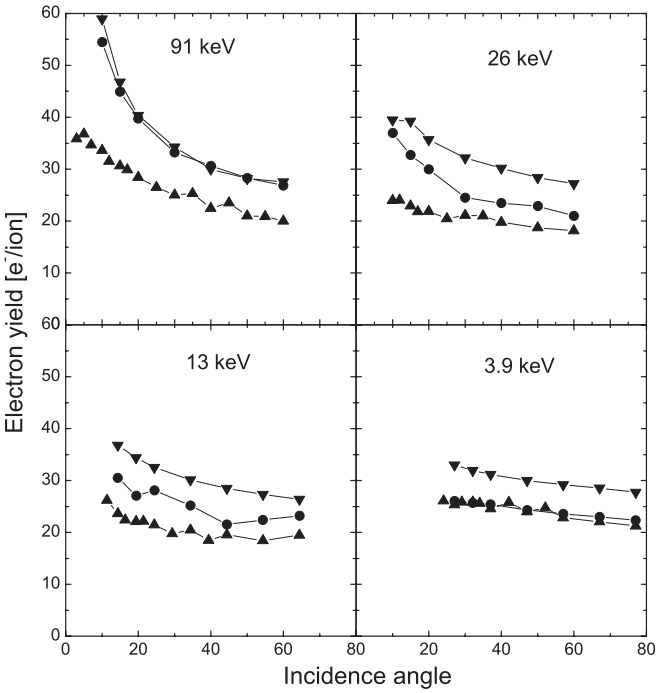

FIG. 7. The electron yield for Au (▲), five monolayers of C_{60} (●), and HOPG (▼) for different kinetic energies as shown.

electrons created in HOPG have a large escape depth, while in the case of a few MLs of C_{60} the ions enter the Au substrate relatively rapidly. This could lead to fewer electrons escaping from below the surface. With increasing kinetic energy, the electron yield on C_{60} starts to differ from that on Au. Upon going to even higher kinetic energies this difference becomes larger, until at 91 keV the electron yields on C_{60} and HOPG are the same. It therefore seems reasonable to assume that in the case of C_{60}, the slope of the kinetic electron emission vs kinetic energy is somewhat steeper than for Au and HOPG.

V. CONCLUSIONS

The secondary electron yields from highly charged Ar ions interacting with clean Au thin films of C_{60} evaporated on Au and bulk HOPG have been determined for various incidence angles and kinetic energies. The angular dependency as a function of the number of MLs of C_{60} show that electron yields increase with C_{60} layer thickness.

Although the characteristic layer thickness Θ_{Ch} is the same for Ar^{4+} and Ar^{13+}, the relative enhancement in electron yield for bulk C_{60} depends on the charge state of the impinging ion. The difference in absolute electron yield is the same for both ions. This indicates that the potential energy is not responsible for the observed increase, but the kinetic energy. The change in absolute electron yield shows a clear $\sin^{-1}(\phi)$ behavior, while for potential emission a relation $\sin^{-a}(\phi)$, with $a \sim 0.5$, is expected [19].

The increase is explained by the fact that the kinetic emission threshold for C_{60} is much lower than the one for Au. This is supported by data for HOPG, which is expected to behave similarly to C_{60}.

For Ar ion energies $\geqslant$10 keV the kinetic electron emission is of such importance that it hampers the observation of the effects of thin films on the hollow-atom phase of interaction. Lower velocities and higher charge states are required to determine the effects of dielectric thin films on a metallic surface on the electron emission in front of the surface as predicted by Lake *et al.* [11].

ACKNOWLEDGMENTS

This experiment was performed at the ZERNIKELEIF part of the distributed LEIF infrastructure. Support received from the European Project ITS LEIF (RII3/026015) is gratefully acknowledged. This work was also sponsored by the Helmholtzzentrum für Schwerionenforschung GmbH (GSI), Germany–KVI University of Groningen collaboration agreement and the FOM-EURATOM association agreement. The Stichting voor Fundamenteel Onderzoek der Materie (FOM) is financially supported by the Nederlandse organisatie voor Wetenschappelijk Onderzoek (NWO). The Austrian part of the work was supported by the Austrian Science Foundation FWF, by Association EURATOM-ÖAW, and by Kommission zur Koordination der Kernfusionsforschung in Österreich (KKKÖ).

[1] J. P. Briand, L. de Billy, P. Charles, S. Essabaa, P. Briand, R. Geller, J. P. Desclaux, S. Bliman, and C. Ristori, Phys. Rev. Lett. **65**, 159 (1990).

[2] A. Arnau, F. Aumayr, P. M. Echenique, M. Grether, W. Heiland, J. Limburg, R. Morgenstern, P. Roncin, S. Schippers, R. Schuch, N. Stolterfoht, P. Varga, T. J. M. Zouros, and H. Winter, Surf. Sci. Rep. **27**, 113 (1997).

[3] F. Aumayr and HP. Winter, *Springer Tracts in Modern Physics*, Vol. 225 (Springer, Berlin, 2007), p. 79.

[4] J. Burgdörfer, P. Lerner, and F. W. Meyer, Phys. Rev. A **44**, 5674 (1991).

[5] A. Bárány and C. J. Setterlind, Nucl. Instr. Meth. B **98**, 184 (1995).

[6] H. Khemliche, T. Schlathölter, R. Hoekstra, R. Morgenstern, and S. Schippers, Phys. Rev. Lett. **81**, 1219 (1998).

[7] H. Khemliche, T. Schlathölter, R. Hoekstra, and R. Morgenstern, Phys. Rev. A **60**, 3800 (1999).

[8] H. Khemliche, C. Laulhé, S. Hoekstra, R. Hoekstra, and R. Morgenstern, Phys. Scripta **T80A**, 66 (1999).

[9] C. Laulhé, R. Hoekstra, S. Hoekstra, H. Khemliche, R. Morgenstern, A. Närmann, and T. Schlathölter, Nucl. Instr. Meth. B **157**, 304 (1999).

[10] E. Bodewits, R. Hoekstra, G. Kowarik, K. Dobes, and F. Aumayr, Phys. Rev. A **84**, 042901 (2011).

[11] R. E. Lake, J. M. Pomeroy, and C. E. Sosolik, Nucl. Instr. Meth. B **269**, 1199 (2011).

[12] F. W. Meyer, S. H. Overbury, C. C. Havener, P. A. Zeijlmans van Emmichoven, J. Burgdörfer, and D. M. Zehner, Phys. Rev. A **44**, 7214 (1991).

[13] S. Cernusca, M. Fürsatz, HP. Winter, and F. Aumayr, Europhys. Lett. **70**, 768 (2005).
[14] E. Bodewits, H. Bekker, A. J. de Nijs, R. Hoekstra, D. Winklehner, B. Daniel, G. Kowarik, K. Dobes, and F. Aumayr, Nucl. Instr. Meth. B **269**, 1203 (2011).
[15] T. Beier, L. Dahl, H.-J. Kluge, C. Kozhuharov, and W. Quint, Nucl. Instr. Meth. B **235**, 473 (2005).
[16] G. Lakits, F. Aumayr, and HP. Winter, Rev. Sci. Instr. **60**, 3151 (1989).
[17] K. Töglhofer, F. Aumayr, and HP. Winter, Surf. Sci. **281**, 143 (1993).
[18] H. Eder, M. Vana, F. Aumayr, and HP. Winter, Rev. Sci. Instrum. **68**, 165 (1997).
[19] W. Meissl, D. Winklehner, F. Aumayr, M. C. Simon, R. Ginzel, J. R. C. López-Urrutia, J. Ullrich, B. Solleder, C. Lemell, and J. Burgdörfer, J. Surf. Sci.: Nanotechnol. **6**, 184 (2008).
[20] C. Lemell, J. Stockl, HP. Winter, and F. Aumayr, Rev. Sci. Instr. **70**, 1653 (1999).
[21] D. Manura and D. Dahl, *SIMION (R) 8.0 User Manual* (Scientific Instrument Services, Ringoes, NJ 08551, 2008); http://simion.com/.
[22] F. Aumayr, H. Kurz, D. Schneider, M. A. Briere, J. W. McDonald, C. E. Cunningham, and HP. Winter, Phys. Rev. Lett. **71**, 1943 (1993).
[23] H. Eder, F. Aumayr, and HP. Winter, Nucl. Instr. Meth. B **154**, 185 (1999).
[24] H. Kurz, F. Aumayr, C. Lemell, K. Töglhofer, and HP. Winter, Phys. Rev. A **48**, 2182 (1993).
[25] W. Meissl, M. Simon, J. C. López-Urrutia, H. Tawara, J. Ullrich, HP. Winter, and F. Aumayr, Nucl. Instr. Meth. B **256**, 520 (2007).
[26] V. Castaldo, J. Withagen, C. Hagen, P. Kruit, and E. Veldhoven, Microsc. Mincroanal. **4**, 624 (2011).
[27] Cernusca, Ph.D. thesis, TU Wien, 2003.